Geophys. J. Int. (2004) **158,** 1024–1040 doi: 10.1111/j.1365-246X.2004.02355.x

Pn tomographic imaging of mantle lid velocity and anisotropy at the junction of the Arabian, Eurasian and African plates

Ali I. Al-Lazki,[1,*] Eric Sandvol,[2] Dogan Seber,[1] Muawia Barazangi,[1] Niyazi Turkelli[3] and Randa Mohamad[4]

[1]*Institute for the Study of the Continents, Snee Hall, Cornell University, Ithaca, New York* 14853, *USA. E-mail: mb44@cornell.edu*
[2]*Department of Geological Sciences, University of Missouri, 101 Geology Building, Columbia, Missouri* 65211, *USA*
[3]*Department of Geophysics, Kandilli Observatory and Earthquake Research Institute, Bogazici University, Istanbul, Turkey*
[4]*Syrian National Seismological Centre, General Establishment of Geology and Mineral Resources, Damascus, Syria*

Accepted 2004 April 21. Received 2004 April 15; in original form 2002 October 16

SUMMARY

The interaction of the Arabian plate with the Eurasian plate has played a major role in building the young mountain belts along the Zagros–Bitlis continent–continent collision zone. Arabia's northward motion is considered to be the primary driving force behind the present-day westerly escape of the Anatolian plate along the North and East Anatolian fault zones as well as the formation of the Turkish and the Iranian plateaux. In this study we mapped *Pn*-wave velocity and anisotropy structures at the junction of the Arabian, Eurasian and African plates in order to elucidate the upper-mantle dynamics in this region. *Pn* is a wave that propagates within the mantle lid of the lithosphere and is often used to infer the rheology and fabric of the mantle lithosphere. Applying strict selection criteria, we used arrival times of 166 000 *Pn* phases to invert for velocity and anisotropy in the region. Using a least-squares tomographic code, these data were analysed to solve simultaneously for both velocity and azimuthal anisotropy in the mantle lithosphere.

We found that most of the continental regions in our study area are underlain by low *Pn* velocity structures. Broad-scale (∼500 km) zones of low (<8 km s^{-1}) *Pn* velocity anomalies underlie the Anatolian plate, the Anatolian plateau, the Caucasus region, northwestern Iran and northwestern Arabia, and smaller scale (∼200 km), very low (<7.8 km s^{-1}) *Pn* velocity zones underlie southern Syria, the Lesser Caucasus, the Isparta Angle, central Turkey and the northern Aegean Sea. The broad-scale low-velocity regions are interpreted to be hot and unstable mantle lid zones, whereas very low *Pn* velocity zones are interpreted to be regions of no mantle lid. The low and very low *Pn* velocity zones in eastern Turkey, northwestern Iran and the Caucasus region may be associated with the latest stage of intense volcanism that has been active since the Late Miocene. The low *Pn* velocity zones beneath the Anatolian plate, eastern Turkey and northwestern Iran may in part be a result of the subducted Tethyan oceanic lithosphere beneath Eurasia. We also found a major low-velocity zone beneath northwestern Arabia and the Dead Sea fault system. We interpret this anomaly to be a possible extension of the hot and anomalous upper mantle of the Red Sea and East Africa rift system. High *Pn* velocities (8.1–8.4 km s^{-1}) are observed to underlie the Mediterranean Sea, the Black Sea, the Caspian Sea, and the central and eastern Arabian plate. Observed *Pn* anisotropy showed a higher degree of lateral variation than did the *Pn* velocity structure. Although the *Pn* anisotropy varies even in a given tectonic region, in eastern Anatolia very low *Pn* velocity and *Pn* anisotropy structures appear to be coherent.

Key words: anisotropy, Arabia, Middle East, *Pn*, tomography, velocity.

1 INTRODUCTION

The study area is located at the junction of the Arabian, Eurasian and African plates. This region encompasses diverse active plate

*Now at: Department of Earth Sciences, Sultan Qaboos University, PO Box 36, PC 123, Alkhod, Oman.

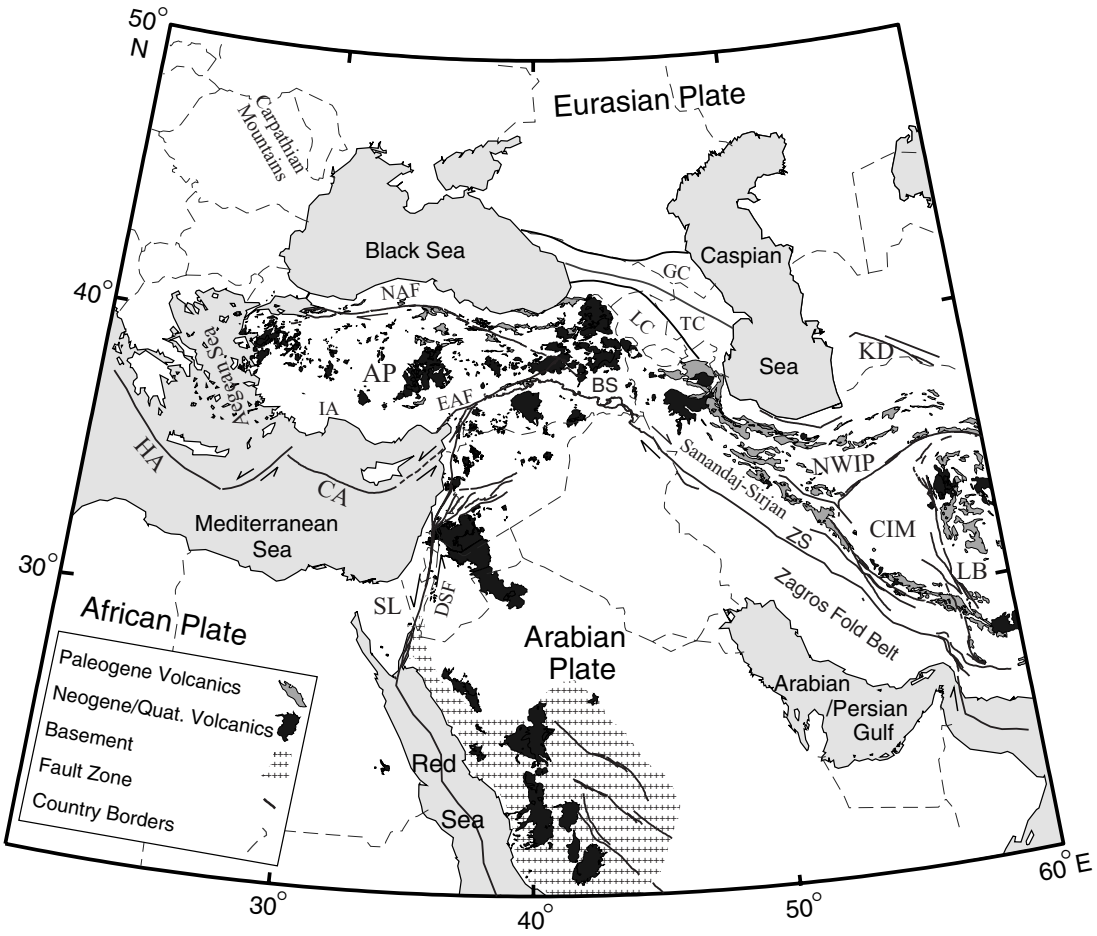

Figure 1. Simplified tectonic map of the study area showing main plate boundaries. AP: Anatolian plate; BS: Bitlis Suture; CA: Cyprean arc; CIM: Central Iranian Microplate; DSF: Dead Sea Fault; EAF: East Anatolian Fault; GC: Greater Caucasus; HA: Hellenic arc; IA: Isparta Angle; KD: Kopeh Dagh; LC: Lesser Caucasus; LB: Lut Block; SL: Sinai and Levantine subplate; NAF: North Anatolian Fault; NWIP: North West Iranian Plate; TC: Transcaucasus; ZS: Zagros Suture.

boundaries and relatively modest active intraplate deformation. Present-day boundaries of the Arabian plate are of several types (Fig. 1). In the southwest, a divergent plate boundary (Red Sea) exemplifies early stages of continental rifting and sea floor spreading. In the northwest, the Dead Sea Fault (DSF) transform system separates the Arabian plate from the Sinai and Levantine subplates (Fig. 1). In the north and northeast the boundary zone is a continent–continent collision, where the Arabian plate is colliding with the Eurasian plate along the Bitlis Suture (BS) and the Zagros Suture (ZS) zones (Fig. 1). Northward motion of Arabia is partially accommodated by the westerly extruding Anatolian plate along the North Anatolian Fault (NAF) and the East Anatolian Fault (EAF) zones (McKenzie 1972; Sengor & Yilmaz 1981; Sengor *et al.* 1985; McClusky *et al.* 2000). The escaping Anatolian plate is bounded in the west and south by the subduction zones of the Hellenic and Cyprean arcs, respectively.

In this paper we use the *Pn* phase to study the mantle lid velocity and infer the state of the lithosphere at the junction of the Arabian, Eurasian and African plates. The *Pn* phase is a guided high-frequency compressional wave that propagates within a high-velocity mantle lid which acts like a waveguide bounded by the low-velocity zone (LVZ) below and the crust above (e.g. Menke & Richards 1980; Beghoul *et al.* 1993). The *Pn*-wave velocity is often used to infer the uppermost mantle rheology. Variations in *Pn* velocities are caused by changes in the physical parameters of uppermost mantle rocks. Changes in temperature and composition and the presence of water and volatiles are the main causes of velocity changes. *Pn* velocities are generally highest in the oceanic lithosphere and could reach up to 8.4 km s^{-1} (Walker 1977). Continental lithosphere *Pn* velocities, however, vary significantly depending on the rheology of the mantle lid. Higher *Pn* velocities (>8 km s^{-1}) imply a tectonically stable mantle lid, while very low *Pn* velocities (<7.8 km s^{-1}) are usually an indication of partial melt (e.g. Hearn 1999; Calvert *et al.* 2000).

Pn velocities also show azimuthal variation. Seismic anisotropy has been observed in the upper mantle in both oceanic (Backus 1965) and continental settings (Beghoul & Barazangi 1990). Earlier studies have concluded that most of the anisotropy occurs in the upper mantle, whereas between 600-km depth and the D″ discontinuity the mantle appears to be relatively isotropic (e.g. Savage 1999; Kendall 2000). Studies of Rayleigh and Love surface waves (e.g. Anderson 1961), shear-wave splitting of phases like SKS (e.g. Silver & Chan 1988), and *Pn* phases (e.g. Hearn 1996; Smith & Ekstrom 1999) have provided abundant evidence for the presence of upper-mantle seismic anisotropy. The major cause of seismic anisotropy in the upper mantle is lattice preferred orientation (LPO) caused by plastic deformation (e.g. Mainprice & Nicolas 1989; Karato 1998). It is well established that the strength of LPO is a function of finite

strain and hence seismic anisotropy should evolve with deformation history (Savage 1999; Mainprice *et al.* 2000).

In a previous study in the same region, Hearn & Ni (1994) used 70 755 *Pn* phases to invert for *Pn* velocities without anisotropy consideration. Their study had good ray coverage within the Aegean region, but in the regions south of the Caspian Sea and within the Arabian plate only sparse data were available. A similar uppermantle study by Hearn (1999) on the uppermost mantle *Pn* velocity and anisotropy of the European region covered only parts of the Aegean Sea. In this study we use a technique similar to that of Hearn (1999) and tomographically invert for *Pn* velocity and anisotropy in the region. This study uses a significantly larger number of seismic stations and events, especially in the Arabian–Eurasian collision zone. The use of the temporary 29-station broadband network of the Eastern Turkey Seismic Experiment and the 20-station short-period seismic network in Syria provides critical and high-resolution data that are crucial in understanding the complex tectonics of this region.

2 TECTONIC BACKGROUND

Along the northern and northeastern boundary of Arabia, the opening of the Neo-Tethys ocean began in the Late Permian and continued until Late Cretaceous times. Consumption of the Neo-Tethys oceanic lithosphere by subduction began in the Early Cretaceous along the eastern and northeastern boundaries of the Arabian–African plate. The timing of collision between Arabia and Eurasia along the BS and the ZS is still being debated, with proposed ages ranging from Late Cretaceous (Takin 1972) to Pliocene (Dewey *et al.* 1973). Hempton (1982, 1985) proposed an initial suturing to have begun in Middle to Late Eocene.

Along the present-day southwestern boundary of the Arabian plate, the opening of the Red Sea and the Gulf of Aden is thought to have occurred in two extensional episodes, one in the Middle–Late Eocene period and the other in the Early Pliocene (e.g. Hempton 1987). This separation of Arabia from Africa is accommodated by the left lateral DSF system and is also considered to be responsible for the reorganization of relative plate motions in the Anatolian plateau (Bozkurt 2001). In the Early Pliocene, continued north–south convergence between Arabia and Eurasia resulted in the extrusion of the Anatolian plate along the NAF and EAF zones (e.g. Sengor & Yilmaz 1981; Sengor *et al.* 1985). The two fault systems separate an eastern domain experiencing mainly north–south compression from the westerly escaping Anatolian plate. The tectonic domains east of the NAF and EAF comprise several sub-domains from north to south: the Greater Caucasus, the Transcaucasus depression, the Lesser Caucasus, the east Anatolian plateau and the Arabian platform (Kocyigit & Erol 2001).

Extension behind the Aegean subduction system began in the Middle to Late Miocene (13–10 Ma) (Le Pichon & Angelier 1979; Jackson 1994) or possibly as recently as 6 Ma (Mckenzie 1978). Extension of up to 100 per cent is thought to have affected the Aegean region in an north–south direction (Mckenzie 1978), with the greatest extensional strains located in the southern Aegean, north of Crete (Angelier *et al.* 1982; Jackson 1994). Present-day extension occurring on the northern Aegean extending to ∼31°E within the Anatolian plate (Angelier *et al.* 1982) is believed to be associated with the retreating subduction of the African oceanic lithosphere (eastern Mediterranean) beneath the Hellenic arc. This extension dies out in the area north of ∼42°N in Bulgaria and northern Greece (Fig. 1).

3 METHOD

P-wave traveltime residuals from sources at 1°.8 to 16° distances were inverted to obtain the uppermost mantle velocity model for the region. A tomography method based on observed traveltime residuals developed by Hearn (1996) was used to invert for *Pn*-wave velocity and anisotropy as well as event and station delays. The model assumes that *Pn* behaves as a diffracted head-wave that travels through the uppermost mantle (a crust layer over a half-space upper mantle). The *Pn* phase model path includes three legs: an event leg, a mantle leg and a station leg. The three segments of *Pn* traveltime path are described by the following traveltime equation (Hearn 1996):

$$t_{ij} = a_i + b_j + \sum d_{ijk}(S_k + A_k \cos 2\Phi + B_k \sin 2\Phi), \quad (1)$$

where a_i is the station time leg for station i, b_j is the event time leg for event j, d_{ijk} is the distance travelled between event j and station i for cell k, Φ is the back azimuth angle, S_k is the slowness value for cell k, and A_k and B_k are anisotropy coefficients for cell k (Hearn 1996). Eq. (1) is solved for all event–station pairs using an LSQR algorithm that solves sparse linear equations and least-squares problems (Paige & Saunders 1982) to obtain slowness, anisotropy, and station and event delays (Hearn 1996). This method then separates traveltimes for each station and event leg using an assumed crust model (this study assumes a model crust thickness of 35 km with 6.2 km s^{-1} velocity) and an average *Pn*-wave velocity of the study area (8.1 km s^{-1}). The average *Pn*-wave velocity was determined from the slope of the linear fit of the screened traveltime data. This method also adjusts for the curvature of the Earth (Hearn 1996). In our inversion we used a cell size of 0°.25 × 0°.25 for the region, similar to previous studies.

Since traveltime data include a certain degree of noise and uneven ray coverage, a damping parameter is used to regularize the solution (Paige & Saunders 1982) and reduce noise artefacts. The use of LSQR damping for both velocity and anisotropy parameters resulted in a relatively smooth image. In our inversion process, after a series of tests, we chose a final damping value of 1000 for both velocity and anisotropy. This value was found to best remove erroneous data noise and best balance the contributions of anisotropy and velocity to the inverted model. Damping values of less than 1000 were found to produce spurious velocity anomalies, while values larger than 1000 significantly reduced our model resolution. Since event locations were fixed in our inversion, we introduced an error range to test the sensitivity of the tomographic model to possible erroneous event locations. This error was added to the events that passed the criteria selections. We found that the range 0°.14−0°.5 showed negligible difference in the anomaly details of the inverted model (see supplemental Fig. S1).

4 DATA

In this study two categories of *Pn* phase data were used. The first category comprises phase data picked by the authors from the Eastern Turkey Seismic Experiment (ETSE) (29 PASSCAL broadband stations), the Syrian National Seismic Network (20 short-period stations), the southern Caspian broadband stations (five stations), the Iranian Long Period Array (ILPA) (five stations), and the Turkish National Network (five short-period stations) data (Fig. 2a). The second category comprises phase data that were extracted from the International Seismological Centre (ISC) and the National Earthquake Information Center (NEIC) earthquake catalogues (Figs 2a and b).

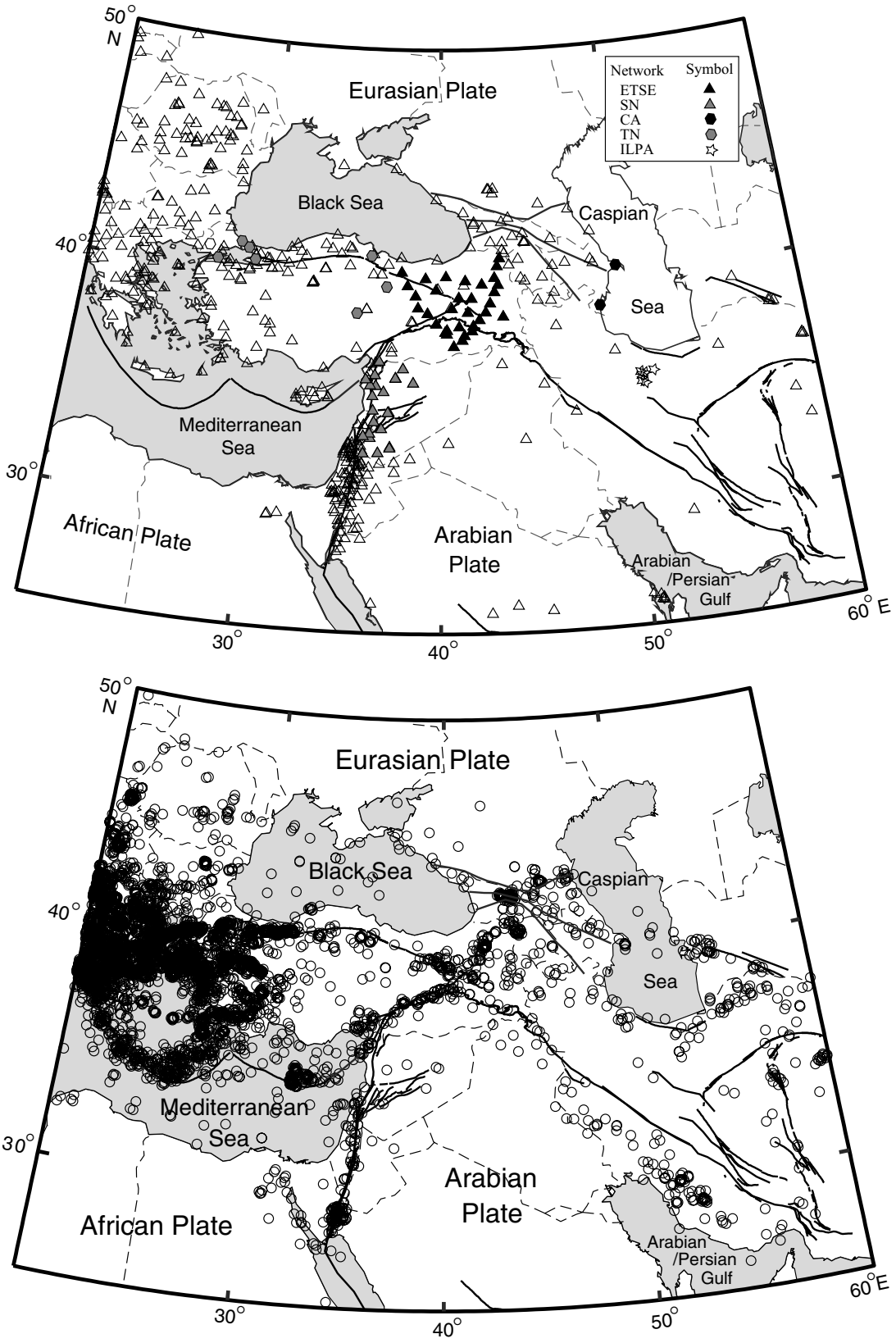

Figure 2. (a) Map showing seismic stations used in this study. CA: southern Caspian Sea stations; ETSE: Eastern Teismic Experiment stations; ILPA: Iran Long Period Array; SN: Syrian National network; TN: Turkish National network. Open triangles correspond to selected stations from the National Earthquake Information Center (NEIC) and the International Seismological Centre (ISC) catalogues. (b) Map showing seismic events (in circles) used in the *Pn* velocity and anisotropy tomography inversion. (See Fig. 1 for geographic locations.)

The second category of *Pn* phase data include 729 819 phases that were extracted from the ISC data catalogue and 95 716 phases from the NEIC data catalogue. A total of 7414 *Pn* phase picks were read by the authors using the data from the ETSE, the Syria network, the ILPA, the Caspian stations and the Turkish network. In addition, ETSE stations (Fig. 2a) were used to locate local seismicity in eastern Turkey. These local events amounted to a total of 2715 phase picks, which provided a dense coverage within the 29-station array (Figs 2a and b).

Since the phase data might include many erroneous readings, especially those obtained from catalogues, a rigorous selection method was used. In assessing data quality and integrity we used 13 criteria to filter out possible erroneous phase data at three levels. To minimize location errors the following criteria were used: locations were selected that had a minimum of 25 stations; azimuth gap $<150^\circ$; rms residuals <10 s; nearest station used in the calculation <800 km. Phase data were iteratively selected so that the inversion used a minimum of five stations to record a single event; a station had to have recorded a minimum of 10 events, with 10-s maximum time residual and an event depth maximum of 45 km. Furthermore, phase data were screened to include only impulsive arrivals, with pick precision less than 2 s. We have experimented with a number of more strict criteria in our ISC and NEIC data and found that, in regions where we maintained sufficient ray coverage and resolution, our resulting model was not affected. For the data picked by the authors we only used phases with estimated accuracy of 1 s or better, in terms of picking precision. Out of 8944 events (Fig. 2b) and their associated stations, a total of 166 000 phases were selected using a maximum of 10-s traveltime residual (Fig. 3a). Our tomographic inversion achieved a 35 per cent variance reduction from the initial linear fit (Fig. 3b).

The station density used in the *Pn* velocity inversion is highly variable in the study area (Fig. 4). High station density areas are located along the DSF system, in eastern Turkey, in and around the Caucasus mountain belts, in and around the Aegean Sea and within the Bulgarian and Romanian territories (Fig. 2a). There is sparse station coverage in the central and northeastern Arabia platform and east of 45°E meridian (Fig. 2a). The highest event density occurred in the Aegean region and the lowest within the Arabian plate (Fig. 2b). The path density for those events recorded at various stations is shown in Fig. 4 as hit counts for each $0.^\circ25 \times 0.^\circ25$ cell. Regions with the highest cell hit counts, >64 hits, cover most of the area west of the Caspian Sea including Turkey, Greece, the Aegean Sea, southern Romania, the eastern Mediterranean Sea and the DSF system (Fig. 4). Areas with fewer ray hits, between 6 and 64 hits, predominate in the rest of the study area in parts of northern Arabia, Iran, the southern Caspian Sea, central and northern Romania, and the central and northern Black Sea (Fig. 4).

5 RESOLUTION ANALYSIS

Although it is customary to discuss resolution analysis after presenting the inversion results, we will start discussing resolution analysis beforehand in order to give the reader a feel for the data resolution capacity in the study area. We used two separate geometries to test the resolution of our tomographic models. These two geometries include a checkerboard and spike tests. We recognize that these two tests may only represent end-members of our model resolution and may be biased toward an apparent higher resolution.

A synthetic checkerboard model ($2^\circ \times 2^\circ$), including a Gaussian random noise of 1-s amplitude, was used to test data coverage resolution using the same damping parameters as the tomographic model inversion. The input synthetic velocity checkerboard (Fig. 5a) was made of alternating high (+0.25 km s^{-1}) and low (-0.25 km s^{-1}) velocity anomalies, while the anisotropy checkerboard (Fig. 6a) was made of alternating east–west and north–south fast directions with 0.25 km s^{-1} magnitude for both orientations.

The velocity checkerboard test results could be categorized into two end-member levels of resolution in the study area. The highest level of resolution is in regions where the shape, magnitude and polarity of the squares are well resolved. This level occurs in the Aegean region and western Turkey. The lowest level of resolution, where no shape, magnitude or polarity is clearly resolved, occurs only in a small portion of the border zone between Iraqi and Saudi Arabian territories and at the model edges (Fig. 5b) due to lack of data coverage in these regions. We have reasonably good resolution of both the shape and magnitude of our test anomalies in central and eastern Turkey. However, our model appears to have poor resolution in central and northern Iran. The resolution is higher in southern and northeastern Iran in regions directly northeast of the Arabian/Persian Gulf (Fig. 5b).

We also tested the resolution of our tomographic model using a spike test with a large null space between each spike. The results from this test were consistent with the results from the checkerboard test (see electronic supplemental Fig. S2).

The two end-member resolution levels also apply to the anisotropy checkerboard test results (Fig. 6b). The highest level of resolution, with complete recovery of shape, magnitude, direction and polarity, occurs within the Aegean region, Greece and western Turkey (Fig. 6b). Reasonably good anisotropy resolution is obtained along the DSF system, central to eastern Turkey, Romania, Bulgaria and the Caucasus region. Within these areas there is some smearing of our test anomalies. One example is the southwestern portion of the EAF zone where anisotropy directions are NE–SW oriented (Fig. 6b). Because anisotropy involves the determination of orientations, it is more prone to smearing effects due to uneven station and event distributions. This is exemplified in northern Iran, where unresolved anisotropy orientations form parallel zones of similar anisotropy orientations along the same areas as the velocity smearing paths (Fig. 6b). A zone with relatively improved shape and orientation resolutions, but smaller magnitudes, occupies the region directly northeast of the Arabian/Persian Gulf.

6 INVERSION RESULTS

6.1 *Pn* velocity anomalies

Pn velocity tomography with an anisotropy component shows two scales of low *Pn* velocity anomalies (Fig. 7a). First, a broader scale ($\sim$500 km) low (<8 km s^{-1}) *Pn* velocity anomaly underlies northwestern Iran, eastern Anatolia, the Caucasus and most of the Anatolian plate. These broad-scale low *Pn* velocity anomalies occupy regions within the Eurasian side of the Eurasia–Arabia collision zone. In central Iran, fast *Pn* velocities appear to extend beyond the ZS line, while in northwestern Iran and eastern Turkey the high *Pn* velocities are limited to the region immediately south of the BS and the EAF zone (Fig. 7a). At the northwestern boundary of the Arabian plate a broad, low *Pn* velocity anomaly underlies the DSF system and western Arabian plate proper (Fig. 7a). Farther south the latter broad anomaly extends to underlie the Sinai and Levantine region (Fig. 7a). The broad low *Pn* velocity anomaly of northwestern Arabia extends only as far north as central and western Syria. Minor

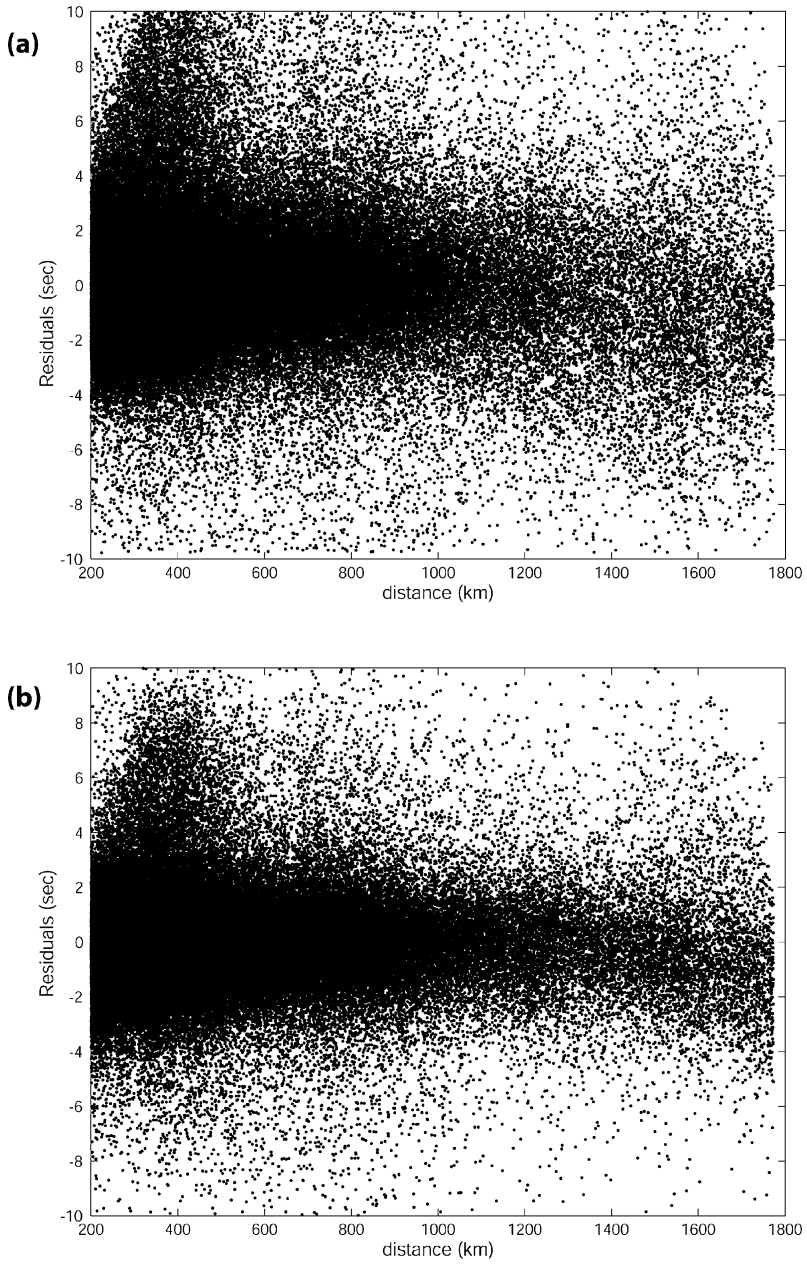

Figure 3. (a) Input traveltime residuals (corrected for a 2-D velocity fit). A 10-s cut-off is used in the *Pn* tomography inversion. The traveltime residuals are calculated using the *Pn* average velocity of the study area (8 km s^{-1}). The large number of positive residuals between 200 and 400 km is most probably misidentified Pg arrivals; we have found that these phase data have little impact on our results (see electronic supplement Fig. S3). (b) Traveltime residuals obtained using the *Pn* tomography results. A 35 per cent variance reduction is obtained compared with the input 2-D fit residuals. (See Fig. 1 for geographic locations.)

low-velocity tongues, partly caused by smearing, extend within the fast velocity zone south of the BS and EAF zone.

Secondly, five smaller scale (∼200 km) anomalies with *Pn* velocities lower than 7.8 km s^{-1} are found to underlie areas within the broader scale low-velocity anomalies. Those shorter scale anomalies occur beneath southernmost Syria and northern Jordan, the Lesser Caucasus, the Isparta Angle and central Turkey. An isolated shorter scale low-velocity anomaly underlies a region in the northern Aegean Sea and parts of westernmost Turkey. Other low *Pn* velocity anomaly zones underlie western Greece, Bulgaria, western Romania and easternmost Yugoslavia (Fig. 7a).

Zones of high *Pn* velocities (8–8.4 km s^{-1}) underlie the interior of the Arabian plate (including the Zagros fold belt), the southern Caspian Sea extending eastward beneath the Kopeh Dagh and westwards beneath Azerbaijan, the Black Sea and most of the eastern Mediterranean Sea. Other regions showing high *Pn* velocity within the broad low-velocity anomalies underlie regions within the Central Iranian Microplate (CIM) and a corridor directly south of the Caspian Sea that extends southwest to the Zagros fold belt (in northern Iran), and two corridors in the eastern and western parts of the Anatolian plate (Fig. 7a). Also, we observe zones of very high *Pn* velocity (>8.2 km s^{-1}) beneath regions directly north of the Hellenic arc, the intersection between the Cyprean and the Hellenic arcs, in eastern Romania, and Azerbaijan (western Greater Caucasus).

We found only subtle differences in *Pn* velocities when not including anisotropy in our tomographic inversion (Fig. 7b). The

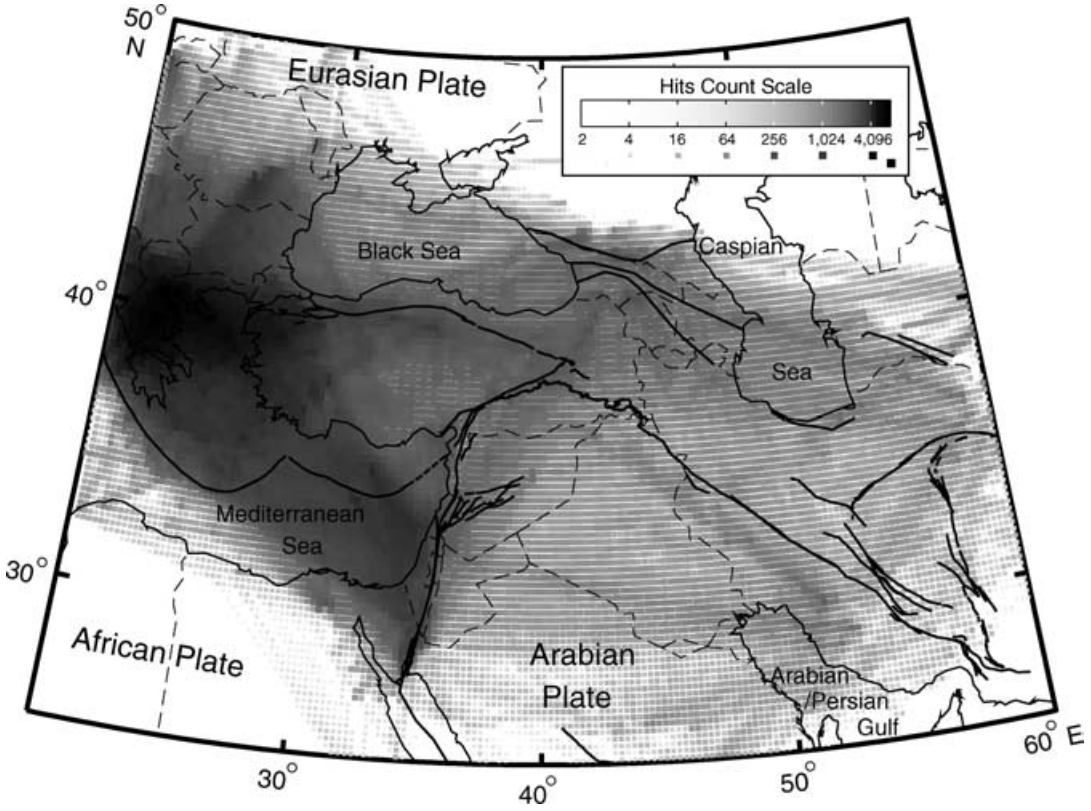

Figure 4. Hit map of the study area using a logarithmic (base 2) grey-scale.

anisotropy effect appears to be strongest under the Anatolian plate, the Aegean Sea, the Hellenic arc and the Black Sea. Generally, including the anisotropy component in the *Pn* velocity inversion focuses anomalies. For example, the shorter scale, very low *Pn* velocity anomaly of the northern Aegean Sea (Fig. 7a) becomes spread out within the Aegean Sea and western Turkey in the isotropic model (Fig. 7b). Including an anisotropy component laterally displaces the anomalies. For example, in the isotropic model (Fig. 7b), the high-velocity anomaly southwest of the Hellenic arc is displaced to the northeast of the Hellenic arc, within the Aegean Sea (Fig. 7a). Similarly, the low-velocity anomaly along western Greece (Fig. 7a) is replaced by a high-velocity anomaly at the corresponding area in the isotropic model (Fig. 7b). Because of the fewer paths in the eastern parts of the study area, we observe no significant differences between the isotropic and anisotropic models. The high-velocity corridor, directly south of the southern Caspian Sea, is caused by including anisotropy (Fig. 7a) in the inversion, and therefore needs to be interpreted cautiously since that region does not show good azimuthal coverage of ray paths.

To test further for possible uncertainties in the inverted anisotropic *Pn* velocity model, we used a bootstrap technique used by Hearn (1996). The bootstrap method iteratively re-samples the data pool and re-runs the inversion using the standard deviation in bootstrapped velocities as proxies for errors of the model. Bootstrap errors for our *Pn* velocity model are typically less than 0.05 km s^{-1} throughout the study area (Fig. 8). Few zones showed errors higher than 0.05 km s^{-1}. Those regions with large errors included the southeastern tip of the Caspian Sea, a small area along the northern Zagros fold belt, and a small area along the NAF zone (Fig. 8).

6.2 *Pn* anisotropy

Fig. 9 shows the resulting anisotropy magnitudes and directions inverted simultaneously with *Pn* velocity. Observed anisotropy magnitudes vary between 0.0 and 0.65 km s^{-1}. The largest anisotropy values occur within the Aegean Sea (∼0.6 km s^{-1}), the Hellenic arc (∼0.65 km s^{-1}) and the southern portion of the Dead Sea fault system (∼0.45 km s^{-1}), and across the easternmost segment of the NAF zone (∼0.5 km s^{-1}). Smaller anisotropy magnitudes (∼0.2 km s^{-1}) are observed within the Arabian plate and the zones east of it (Fig. 9). These variations in anisotropy magnitude could be due in part to the uneven data coverage (i.e. we have damped our inversion in such a way that regions with poor resolution tend to have smaller anisotropy magnitudes).

Unlike the tomographic velocity anomalies, observed anisotropy anomalies show a higher degree of lateral variability. We observed sudden anisotropy changes across plates and along plate boundaries. Since not all anisotropy values are well resolved, we will address only those regions with good anisotropy resolution. Within the Anatolian plate anisotropy fast axes are predominantly east–west in the east, north–south at the centre and east–west in western Turkey. Similar sudden changes in anisotropy are observed along the DSF system, where two different trends of anisotropy orientations are observed (Fig. 9). A predominantly east–west fast anisotropy orientation is present along the northern parts of the DSF system. A NE–SW anisotropy orientation is imaged along the southern portion of the DSF system. Anisotropy orientations along the DSF system show consistency along a narrower band in the inland regions. This contrasts with wider zones of consistency in the Mediterranean Sea side (Fig. 9). The zone parallel to the restraining bend of the DSF

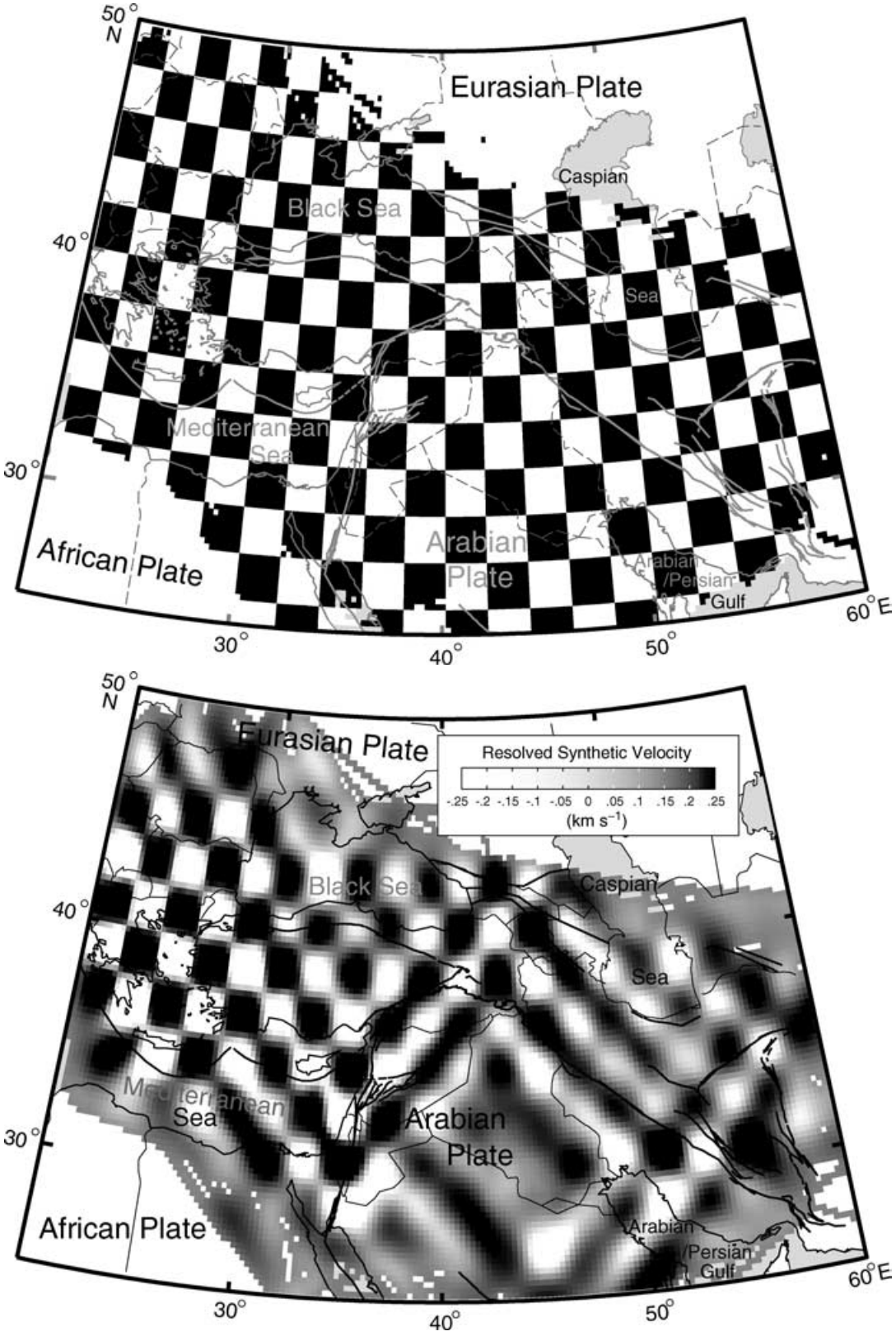

Figure 5. (a) Checkerboard synthetic velocity anomalies used to test the ability of the available stations and events coverage to resolve a 2° × 2° velocity square. The anomaly amplitudes alternate between −0.25 and +0.25 km s^{-1} velocity. (b) *Pn* velocity checkerboard test result. (See Fig. 1 for geographic locations.)

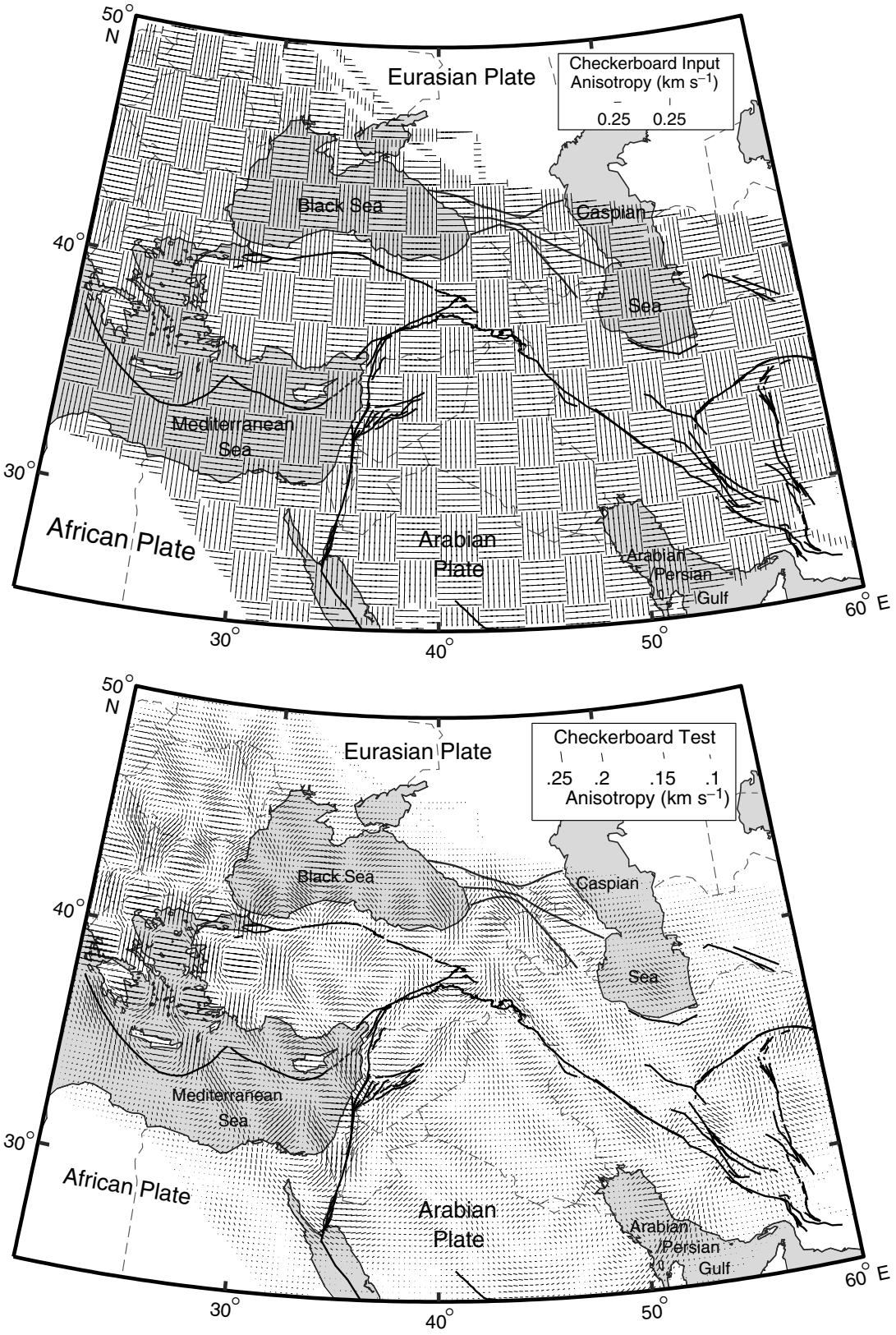

Figure 6. (a) Checkerboard synthetic anisotropy anomalies used to test the ability of available stations and events coverage to resolve a 2° × 2° anisotropy square. The squares are made of alternating north–south and east–west anisotropy orientations of 0.25 km s^{-1} magnitude. (b) *Pn* anisotropy checkerboard test result. (See Fig. 1 for geographic locations.)

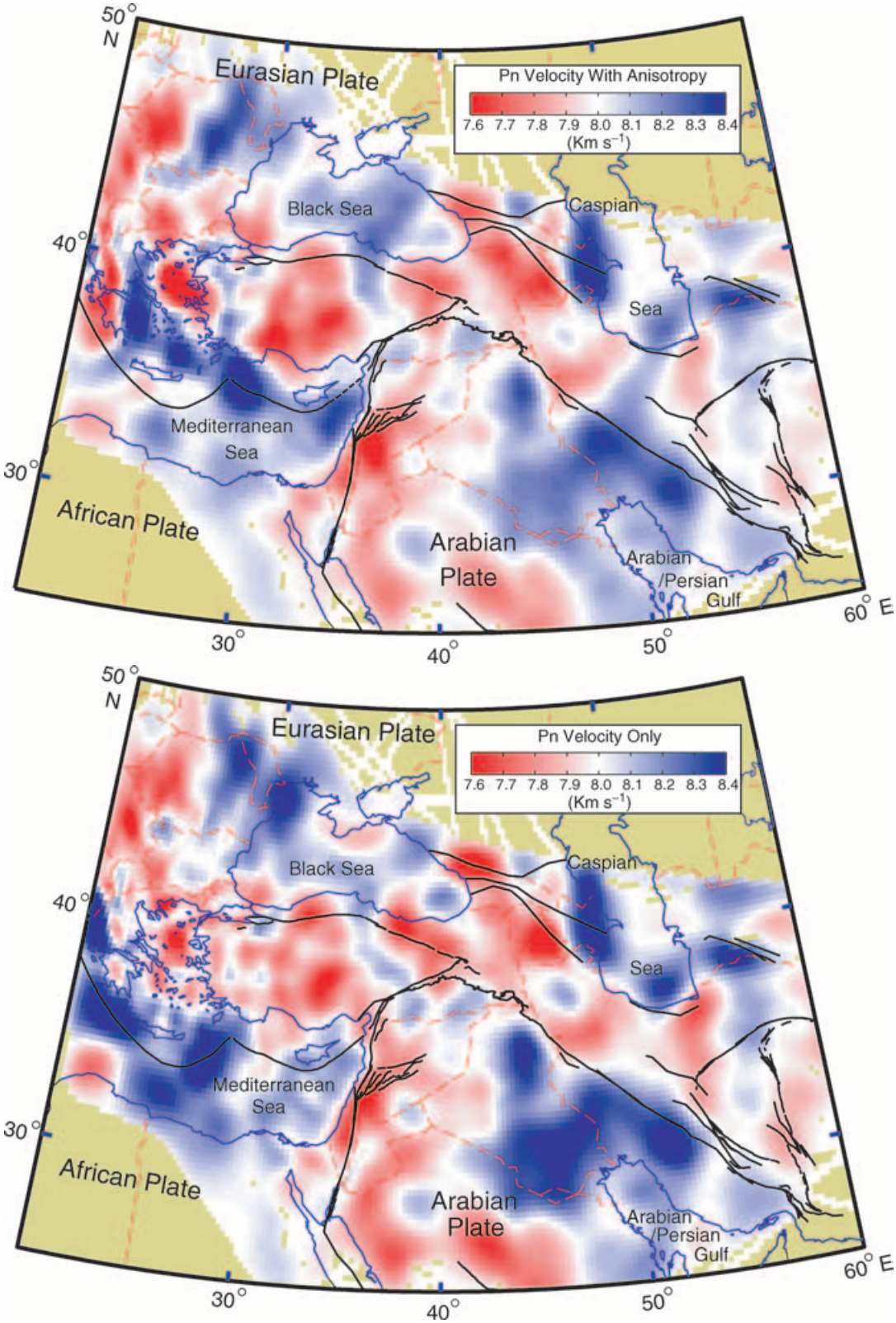

Figure 7. (a) A map showing the *Pn* velocity tomographic results including *Pn* anisotropy. The image shows a broader scale low *Pn* velocity (<8 km s^{-1}) anomaly underlying the boundary zone of Arabia and most of the Anatolian plate. Within the broader low-velocity zone anomalies, shorter scale very low *Pn* velocity (<7.8 km s^{-1}) anomalies underlie southern Syria, the Lesser Caucasus region, the Isparta Angle and central Turkey. (b) A map showing the optimal isotropic *Pn* velocity model. This model shows minor differences from the anisotropic model of panel (a). Notice the difference in the Aegean Sea region, where higher velocities south of the Hellenic arc are displaced northward inside the Sea of Crete and southern Aegean Sea. (See Fig. 1 for geographic locations.)

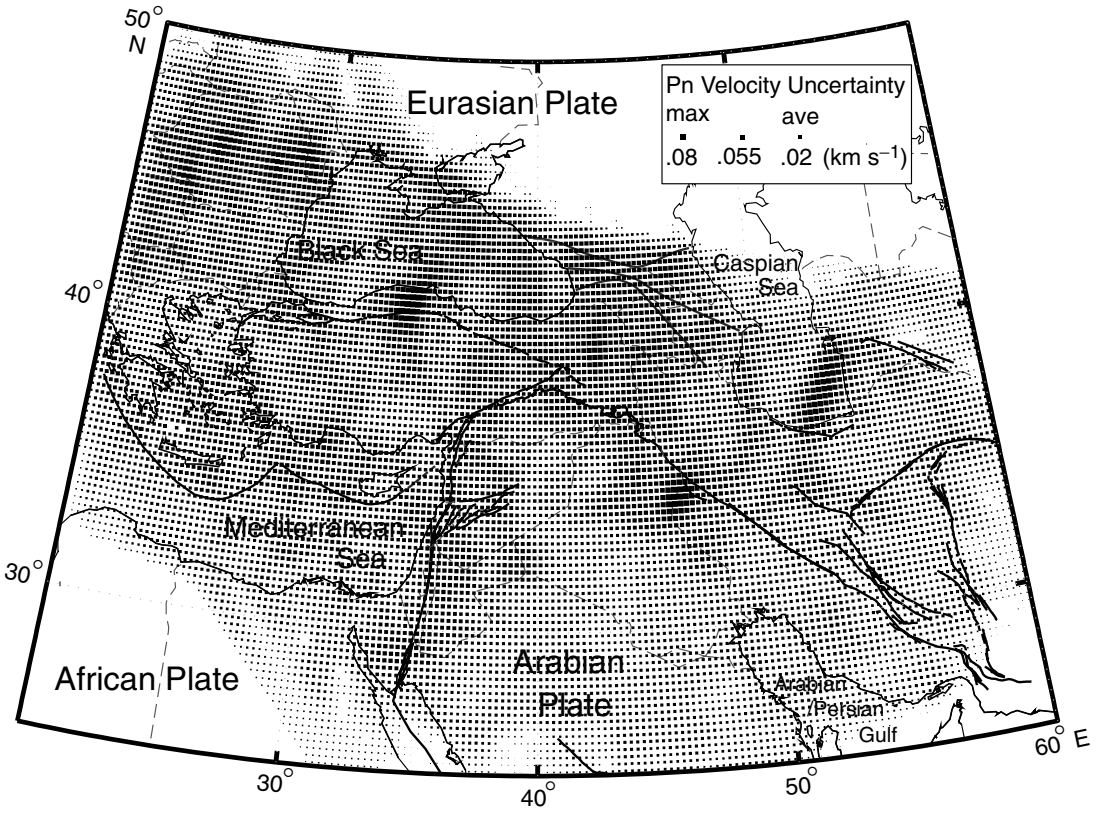

Figure 8. A map showing *Pn* velocity errors calculated using 100 bootstrap iterations. (See Fig. 1 for geographic locations.)

system in southern Syria marks the change in anisotropy orientation from a NE–SW orientation e south to an east–west orientation in the north (Fig. 9). East of the DSF, in the central Arabia platform and along the northern Zagros fold belt, the anisotropy orientations are regarded as erroneous due to the limited ray coverage (Fig. 9).

The Aegean region shows considerable variation in anisotropy orientation. In the south, anisotropy orientations are parallel to the Hellenic arc (arc parallel anisotropy). Within the Aegean Sea, anisotropy is predominantly north–south oriented except for a zone in the northern Aegean Sea, where anisotropy is NW–SE oriented. In eastern Greece and farther southeast in the Aegean Sea, anisotropy is NE–SW oriented. The Sea of Crete shows the smallest anisotropy magnitudes, predominantly east–west oriented.

The overall tomographic azimuthal *Pn* anisotropy shows reasonable correlation with azimuthal anisotropy obtained based on the two-station method (Smith & Ekstrom 1999) in the Aegean region, in the DSF region and in central and eastern Turkey.

We applied a bootstrap error analysis on observed *Pn* anisotropy as well. Comparably low (<0.05 km s^{-1}) errors are also observed for the anisotropy. This may be due to the fact that we used the same damping on both velocity and anisotropy solutions.

6.3 *Pn* station delays

Assuming excellent ray coverage, station delays contain the integrated information about the crustal thickness and average velocity variation of the crust (Fig. 10). Considering that the delay is due to the crustal structure near the station, a station delay of ± 1 s corresponds to $\sim$10 km difference in crustal thickness or $\sim$0.7 km s^{-1} velocity difference from the assumed crustal velocity model. Station delays obtained in our inversion varied between -3 and $+3$ s. Anomalous station delays in excess of 3 s are observed at a few stations and may indicate systematic phase picking errors and/or systematic clock problems at those stations (Grand 1990; Hearn 1996).

Clusters of systematic positive, negative or mixed station delays observed in different regions of the study area may bear some information about the crustal structure (Fig. 10). Positive station delays are mainly indicative of thick and/or slow crust compared with the assumed model. Regions showing clusters of positive station delays are located along the northern segment of the DSF system, in eastern Turkey (mostly ETSE stations), along the Cyprean and the Hellenic arcs, and within Romanian territory (Fig. 10). Negative station delays are indicative of a thin and/or fast crust compared with the assumed model. Zones with negative station delay clusters are those found in the northern Aegean Sea and areas around it including eastern and northern Greece and northwestern Turkey (around the Sea of Marmara), and along the southern portion of the DSF system (Fig. 10).

7 DISCUSSION AND CONCLUSIONS

7.1 Rheology and structure

The *Pn* velocity results provide detailed insight into the rheology and dynamics of the mantle processes in the region. High (>8 km s^{-1}) *Pn* velocity zones found in portions of Arabia and the Mediterranean, Black and Caspian Seas are used to infer the presence of stable mantle lid in these regions. Low *Pn* velocities found beneath

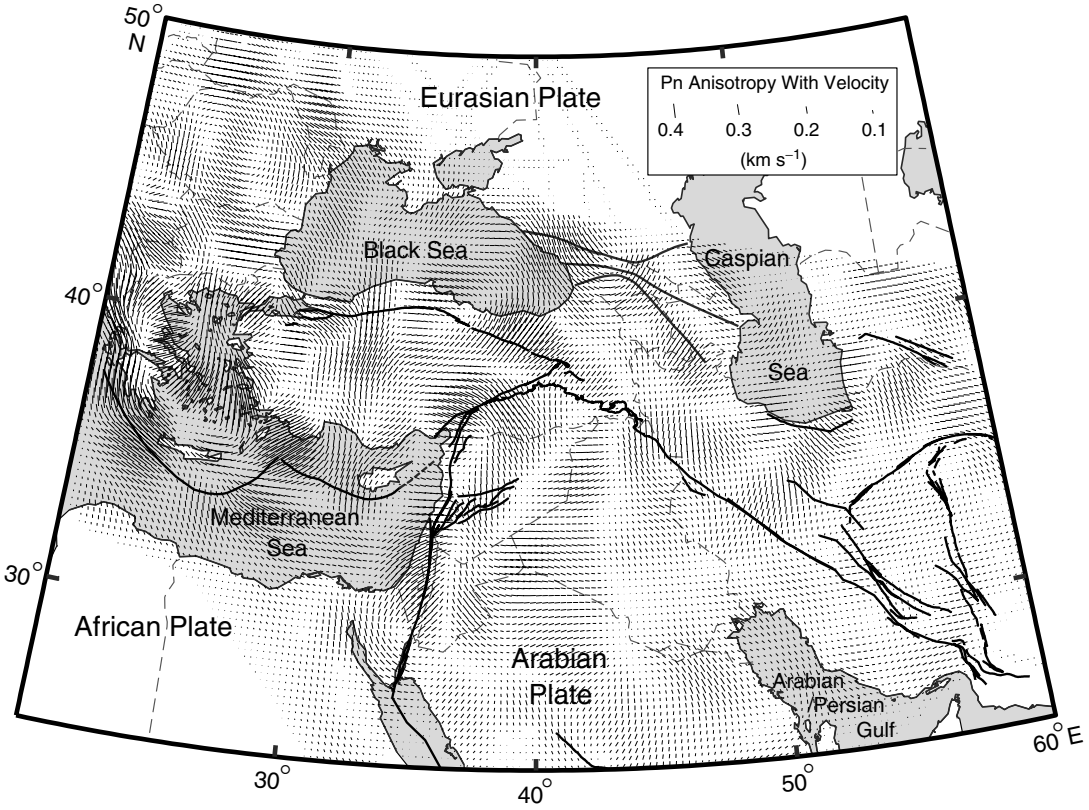

Figure 9. A map showing *Pn* azimuthal anisotropy orientations. Compared with the *Pn* velocity of Fig. 7(a), *Pn* anisotropy orientations display a higher degree of lateral variation in the region. (See Fig. 1 for geographic locations.)

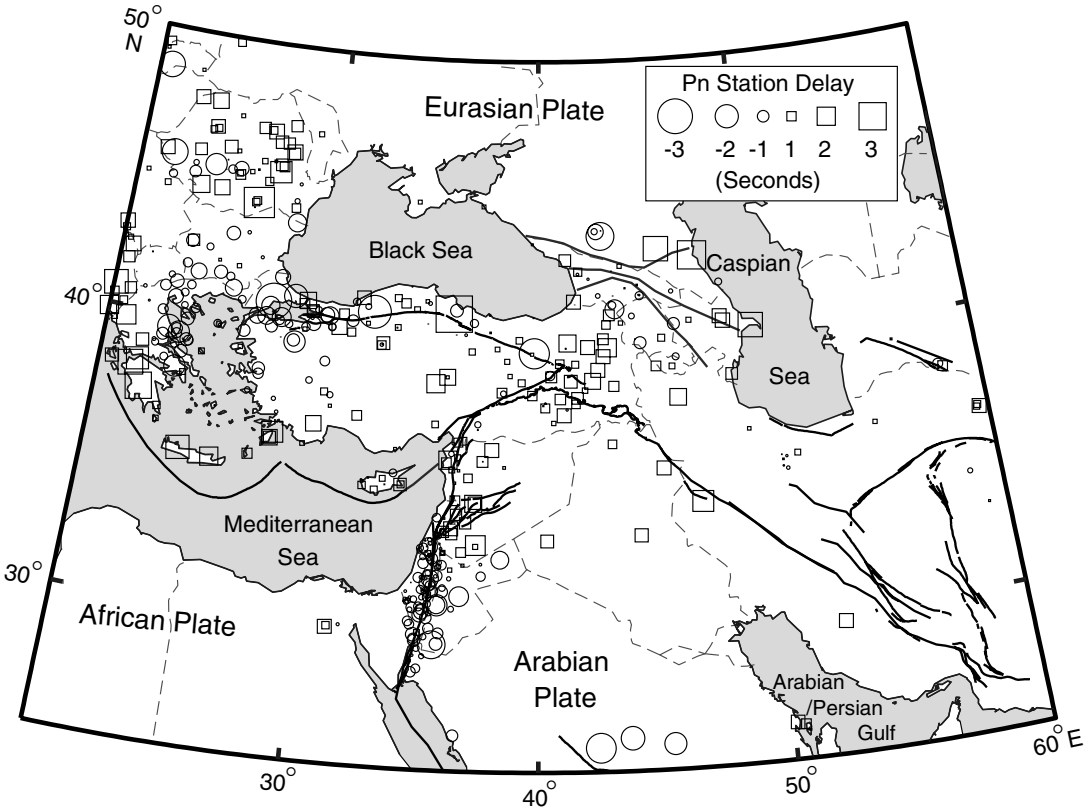

Figure 10. A map showing station delay. Squares represent thick and/or slow crust; circles represent fast and/or thin crust. (See Fig. 1 for geographic locations).

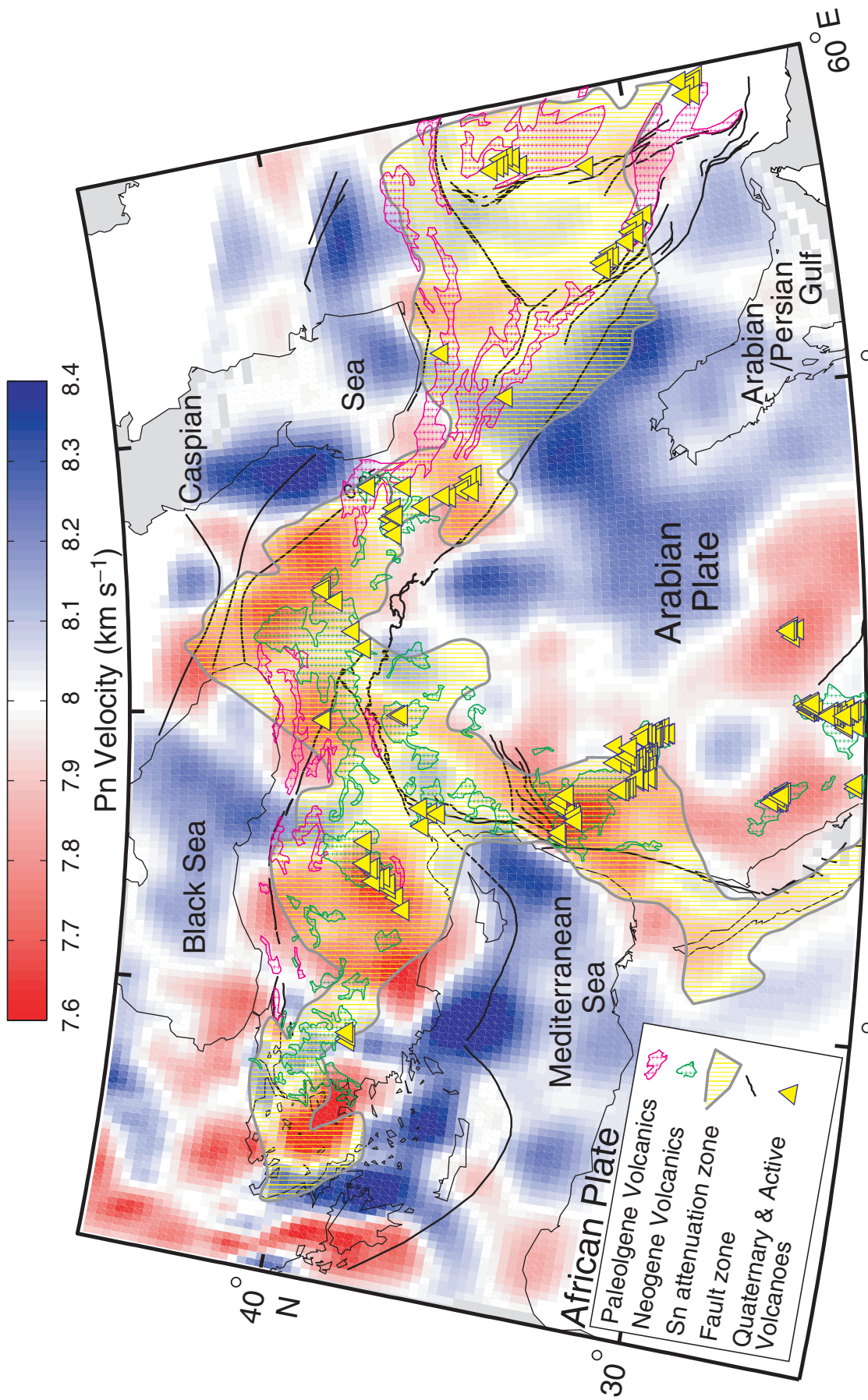

Figure 11. A comparative map showing *Pn* velocity with anisotropy (base map, red–blue colour, see Fig. 7a), volcanic outcrops as green and pink polygons filled with plus signs, *Sn* attenuation zones as yellow hatched areas enclosed by a solid grey line (after Khaled Al-Damegh, personal communication), and volcanoes as yellow triangles. (See Fig. 1 for geographic locations.)

the junction of the Arabian, Eurasian and African plates are used to infer the presence of an anomalously hot and/or thin mantle lid (Fig. 11). The broad-scale, low *Pn* velocity anomalies beneath northwestern Iran, the Caucasus and eastern Anatolia are interpreted to originate from a different geodynamic process from the low *Pn* velocity anomaly beneath the northwestern Arabia plate (Fig. 11). The regions of the Lut Block (LB) and the CIM are associated with volcanic activity throughout the Palaeogene and most of the Neogene (Figs 1 and 11). However, a later stage of volcanic activity in eastern Turkey and northwestern Iran is known to have started in the Late Miocene and continued to historical times (e.g. Yilmaz 1990; Keskin *et al.* 1998). This volcanic activity is possibly related to earlier subduction of the Neo-Tethys oceanic lithosphere. A lithospheric delamination event in Plio-Quaternary time may also significantly contribute to the observed widespread volcanism. Such processes may explain the anomalous nature of the lithosphere in these regions. Within the broad low *Pn* velocity anomalies, zones of high *Pn* velocity (implying a stable mantle lid) underlie the central CIM, a corridor directly south of the Caspian Sea, and a small area in northwestern Iran (Figs 1 and 11). The corridor directly south of the Caspian Sea is observed only in the model with anisotropy and therefore should be considered cautiously because of the poorly resolved anisotropy in that region (Figs 6b and 7b).

A careful examination of the boundary of the high *Pn* velocity zone beneath the southern Zagros region shows that the high-velocity area extends for ∼100 km northeast of the ZS line (Figs 11 and 7a). We interpret this region of high *Pn* velocity possibly to indicate that stable Arabia is underthrusting the southern parts of the Sanandaj–Sirjan region (Eurasia). This interpretation is in agreement with Snyder & Barazangi (1986) who concluded that Arabia is being underthrust beneath the southern parts of the Sanandaj–Sirjan region. The checkerboard resolution tests, however, in this region show that our spatial resolution is poor, and hence this interpretation may be speculative. Farther north the high *Pn* velocity zone underlies only regions directly south of the Zagros–Bitlis suture line. We are confident based on our resolution tests that, in the northern parts of the Zagros–Bitlis region, underthrusting of Arabia is very limited or absent as evidenced by a sudden change in *Pn* velocities across the suture line.

One of the most important results of this study is the discovery of a low *Pn* velocity zone beneath the DSF system and the northwestern Arabian plate. Sandvol *et al.* (2001a) showed that *Sn* is attenuated beneath the entire DSF system, but the extent and location of the anomaly were ambiguous because of limited resolution. In this study, we use the better event–station distribution in the region to quantify the mantle lid velocity beneath northwestern Arabia and the DSF system. We find that the broad, low *Pn* velocity anomaly is not centred along the DSF system, but rather extends a considerable distance within the Arabian plate proper. Also, the very low *Pn* velocity anomaly beneath southern Syria and northern Jordan is located east of the DSF system axis. The anomalous low *Pn* velocity zone is asymmetrical relative to the DSF. Whether or not this anomalous lithospheric mantle is a direct result of the development of the DSF system is arguable. We argue against this possible interpretation owing to the asymmetry of the velocity anomaly with respect to the DSF plate boundary and its extent eastward beneath the northwestern Arabia plate proper. The broad low *Pn* velocity zone underlying the DSF system and northwestern Arabia coincides at the surface with relatively young volcanic outcrops (Neogene/Quaternary), while the very low *Pn* velocity (7.6 km s^{-1}) anomaly is overlain by Quaternary and Holocene volcanoes. We interpret the low *Pn* velocity anomaly beneath the DSF system and northwestern Arabia as a possible northward extension of the anomalous mantle beneath the Red Sea spreading system. This broad region of thin, hot mantle lithosphere may have facilitated the development of the DSF system in the Neogene.

The presence of partial melt lowers normal lithospheric mantle velocities by at least 5–6 per cent (Sato *et al.* 1989). If we are to consider that 8.2 km s^{-1} is the normal *Pn* velocity, then a 6 per cent lower *Pn* velocity would allow us to consider the smaller scale very low *Pn* velocity anomalies beneath southern Syria, the Isparta Angle, central Turkey, the Lesser Caucasus and the northern Aegean Sea as zones of possible partial melt, i.e. the lithospheric mantle is absent (Fig. 11). These very low *Pn* velocity anomalies correspond at the surface with Holocene volcanoes (Fig. 11). The very low *Pn* velocity (7.5 km s^{-1}) centred at the northern Aegean Sea is a region where the largest present-day extensional strain rates are observed (Sonder & England 1989; McClusky *et al.* 2000). The northern Aegean back-arc extension region extends up to ∼42°N and 31°E (Angelier *et al.* 1982; Jackson 1994), which is inclusive of the small very low *Pn* velocity anomaly. The very low *Pn* velocity (∼7.5 km s^{-1}) and the thinned crust (26–32 km) beneath the Aegean (Makris & Vees 1977) are comparable to a rift system, such as the East African rift system beneath Lake Turkana (Keller *et al.* 1994). This very low *Pn* velocity reflects perhaps a very thin to absent mantle lid, where *Pn* propagation is actually sampling asthenospheric rather than lithospheric mantle.

Regions showing stable upper mantle (high *Pn* velocities) underlie central and eastern Arabia, the southern Caspian Sea extending eastward beneath the Kopeh Dagh and westward underlying most of Azerbaijan (eastern Greater Caucasus), most of the Black Sea, eastern portions of the Mediterranean Sea, the Sea of Crete and the southern Aegean Sea (Fig. 7a). The Zagros fold belt is underlain by fast *Pn* velocity (Fig. 7a). This is not surprising since the Zagros fold belt is geologically an integral part of the leading edge of the Arabian plate. We also observed zones of very high *Pn* velocity (>8.3 km s^{-1}) beneath regions directly north of the Hellenic arc, the intersection between the Cyprean and the Hellenic arcs, in eastern Romania, and in Azerbaijan (western Greater Caucasus). Finally, zones of high *Pn* velocity indicative of stable upper mantle form corridors that divide the Anatolian plate into eastern, central and western regions, all of which are underlain by low and very low *Pn* velocity zones (Figs 7a and 11). The origin and cause of these stable mantle lid corridors are unclear, but the location of the corridor at ∼30°E (Fig. 11) coincides at the surface with the easternmost limit of the region undergoing extension in western Turkey and the northern Aegean Sea region.

To analyse our *Pn* tomography results further, we utilized available *Sn* phase attenuation in the region. *Sn* is the shear wave analagous to the *Pn* phase travelling within the lithospheric mantle (mantle lid), but it is more sensitive to temperature and the presence of melt. Fig. 11 shows that zones of high *Sn* attenuation (Khaled Al-Damegh, private communication) correlate spatially with zones of low and/or very low *Pn* velocity.

7.2 *Pn* anisotropy and station delays: tectonic implications

Upper mantle seismic anisotropy is generally attributed to the alignment of olivine (the dominant upper mantle mineral) crystal axes in LPOs (Ismail & Mainprice 1998). In this study *Pn* anisotropy shows more lateral variation than does observed *Pn* velocity (Fig. 12). To avoid interpreting artefacts and smearing effects on observed anisotropy orientations, we will focus our interpretations on the

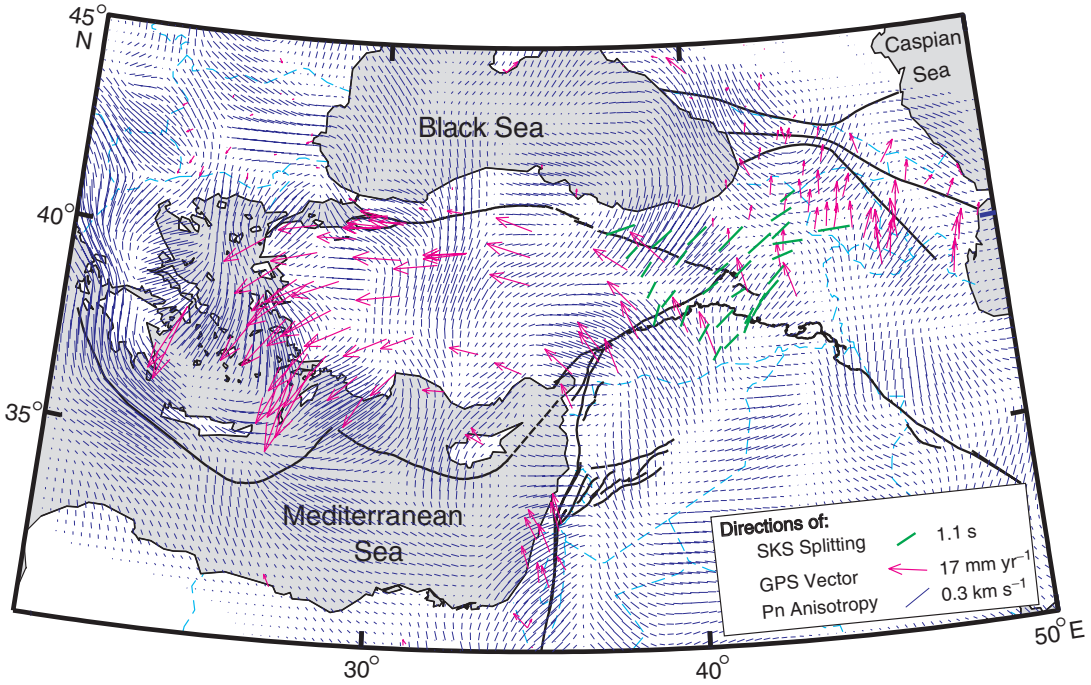

Figure 12. A comparative map showing *Pn* anisotropy in solid blue lines (see Fig. 9), SKS shear wave splitting in solid green lines (after Sandvol *et al.* 2001b), and GPS vector direction in solid pink arrows (after McClusky *et al.* 2000). (See Fig. 1 for geographic locations.)

Anatolian plate, northwestern Arabia, the Aegean region and the eastern Mediterranean Sea, where anisotropy structure is better resolved. In regions such as the Isparta Angle and the northern Aegean Sea, zones of very low *Pn* velocity anomalies showed spatial correlation with zones of distinct and localized *Pn* anisotropy orientations in the same region. At the convergent boundary between the African and Anatolian plates, *Pn* anisotropy is parallel to the arc trend (arc parallel) between the Hellenic trench and its arc extending to ∼40°N, while no clear arc parallel anisotropy is observed south of the Cyprean arc (Fig. 12).

Along the major strike-slip faults of the region (i.e. the NAF and DSF), anisotropy also changes significantly along the strike. Anisotropy orientations along the NAF change from NE–SW in the east, to east–west and north–south in the central parts, and to NW–SE in the west close to the Sea of Marmara. Similarly, the NE–SW oriented fast axis in the southern portion of the DSF changes to an east–west orientation north of the restraining bend of the DSF. This change in anisotropy orientation at the restraining bend coincides with changes in the polarity of station delays (Figs 10 and 12), where the southern segment shows negative station delays and the northern segment shows positive station delays (Fig. 10). The negative station delays clustered along the southern segment of the DSF system may partly be due to a thinned crust. The systematic change of both station delay clusters and anisotropy orientations might suggest that similar processes (influencing station delays) influence anisotropy orientations at depth. The station delays for the entire region are shown in Fig. 10. Although these delays can be used as a first-order indication for crustal thickness and/or velocity variation in the crust, a cautious approach is needed in interpreting these results as noise, and site effects may also influence the results.

While *Pn* anisotropy is a measure of azimuthal anisotropy in the uppermost mantle, shear wave (SKS) splitting results available in the region provide polarization anisotropy information within the entire upper mantle. Fast SKS shear wave splitting determined for ETSE stations in eastern Turkey and a station in central Turkey (Sandvol *et al.* 2001b) generally showed NE–SW fast orientations, while a station in the southern segment of the DSF system showed north–south orientation (Fig. 12). Along the NAF zone and farther southeast in eastern Turkey, azimuthal *Pn* anisotropy matched polarized anisotropy of SKS fast splitting orientations, while no obvious match is observed in the rest of the ETSE stations. NE–SW anisotropy orientations surrounding the easternmost segment of the NAF also correspond with a zone of relatively very low *Pn* velocity (Figs 11 and 12). This implies a thinned or absent mantle lid in the region surrounding the easternmost portion of the NAF and farther southeast directly north of the BS, and that *Pn* anisotropy and SKS splitting are both sampling asthenospheric deformation. While SKS orientations in central Turkey show a very good match with *Pn* azimuthal anisotropy, the stations along the southern segment of the DSF system show clear discrepancy.

We also used available global positioning system (GPS) measurements in the region to possibly relate observed surface plate motion with *Pn* anisotropy orientations. Eurasia fixed GPS vector directions (McClusky *et al.* 2000) within the Anatolian plate do not show a clear relationship with observed *Pn* anisotropy orientations (Fig. 12). The observed sudden variation of *Pn* anisotropy orientation beneath the Anatolian plate contrasts with the relatively uniform GPS-observed westward motion of the Anatolian plate.

Within the Aegean Sea, north–south oriented anisotropy conforms to observed north–south extension of the Aegean region (Mckenzie 1978; Jackson 1994). This suggests that the observed anisotropy orientations within the mantle of the Aegean are influenced by the dynamics of back-arc processes beneath the Aegean Sea.

The lack of simple and consistent correlation between plate motion and *Pn* anisotropy orientations possibly suggests that more complex processes seem to influence *Pn* anisotropy orientations within the mantle lid. These processes could include both crustal (nearby

dominant tectonic stresses) and upper mantle deformation (e.g. mantle flow). This interpretation is based on the following observations: (1) anisotropy orientations that appear to be localized in regions underlain by very low *Pn* velocity zones (e.g. the northern Aegean and the Isparta Angle); (2) anisotropy orientations along the easternmost segment of the NAF zone that are possibly sampling a larger scale asthenospheric anomaly beneath a thin to absent mantle lid; and (3) rapid anisotropy variation.

ACKNOWLEDGMENTS

The authors are grateful for the help and assistance of our colleagues E. Zor, R. Gok, T. Bekler, S. Kuleli, S. Gallow, K. Al-Damegh, G. Brew, A. Calvert, C. Brindisi, F. Gomez, N. Al-Riyami, A. Al-Rumhi and A. Al-Saidi. Special thanks to T. Hearn for his help and assistance in using the *Pn* tomography code. We are thankful for the help of the federal and local governments of Turkey during the installation of our seismic network. We also acknowledge the very helpful field assistance provided by the engineers of the IRIS/PASSCAL Instrument Center at New Mexico Tech. This research is supported by the National Science Foundation (Grant No. EAR-9804780) and Bogazici University Research Fund (Grant No. 99T206).

SUPPLEMENTARY MATERIAL

Figs S1 to S3 are available online at http://www.blackwellpublishing.com/products/journals/suppmat/GJI/GJI2355/GJI2355sm.htm.

REFERENCES

Anderson, D.L., 1961. Elastic wave propagation in layered anisotropic media, *J. geophys. Res.,* **66,** 2953–2963.

Angelier, J., Lyberis, N., Le Pichon, X. & Huchon, P., 1982. The tectonic development of the Hellenic arc and the Sea of Crete: A synthesis, *Tectonophysics,* **86,** 159–196.

Backus, G.E., 1965. Possible forms of seismic anisotropy of the uppermost mantle under oceans, *J. geophys. Res.,* **70,** 3429–3439.

Beghoul, N. & Barazangi, M., 1990. Azimuthal anisotropy of velocity in the mantle lid beneath the Basin and Range Province, *Nature,* **348,** 536–538.

Beghoul, N., Barazangi, M. & Isacks B.L., 1993. Lithospheric structure of Tibet and western North America; mechanisms of uplift and a comparative study, *J. geophys. Res.,* **98,** 1997–2016.

Bozkurt, E., 2001. Neotectonics of Turkey—a synthesis, *Geodyn. Acta: Eur. J. Geodynamics,* **14,** 3–30.

Calvert, A., Sandvol, E., Seber, D., Barazangi, M., Vidal, F., Alguacil, G. & Jabour, N., 2000. Propagation of regional seismic phases (Lg and Sn) and Pn velocity structure along the Africa-Iberia plate boundary zone: tectonic implications, *Geophys. J. Int.,* **142,** 384–408.

Dewey, J.F., Pitman, W.C., Ryan, W.B.F. & Bonnin, J., 1973. Plate tectonics and the evolution of the Alpine system, *Geol. Soc. Am. Bull.,* **84,** 3137–3180.

Grand, S.P., 1990. A possible station bias in traveltime measurement reported to ISC, *Geophys. Res. Lett.,* **17,** 17–20.

Hearn, T.M., 1996. Anisotropic Pn tomography in the western United States, *J. geophys. Res.,* **101,** 8403–8414.

Hearn, T.M., 1999. Uppermost mantle velocities and anisotropy beneath Europe, *J. geophys. Res.,* **104,** 15 123–15 139.

Hearn, T.M. & Ni, J.F., 1994. *Pn* velocities beneath continental collision zones: the Turkish–Iranian Plateau, *Geophys. J. Int.,* **117,** 273–283.

Hempton, M.R., 1982. The North Anatolian Fault and complexities of continental escape, *J. Struct. Geol.,* **4,** 502–504.

Hempton, M.R., 1985. Structure and deformation history of Bitlis suture near Lake Hazar, southeastern Turkey, *Bull. geol. Soc. Am.,* **96,** 233–243.

Hempton, M.R., 1987. Constraints on Arabian plate motion and extensional history of the Red Sea, *Tectonics,* **6,** 687–705.

Ismail, W.B. & Mainprice, D., 1998. An olivine database: An overview of upper mantle fabrics and seismic anisotropy, *Tectonophysics,* **296,** 145–157.

Jackson, J., 1994. Active tectonics of the Aegean region, *Annu. Rev. Earth Planet. Sci.,* **22,** 239–271.

Karato, S.-I., 1998. Seismic anisotropy in the deep mantle, boundary layers and the geometry of mantle convection, *Pure appl. Geophys.,* **151,** 565–587.

Keller, G.R. *et al.*, 1994. The East African Rift system in the light of KRISP 90, *Tectonophysics,* **236,** 465–483.

Kendall, J.-M., 2000. Seismic anisotropy in the boundary layers of the mantle, in, *Earth's Deep Interior: Mineral physics and tomography from the atomic to the global scale,* American Geophysical Union, Geophysical Monograph, **Vol. 117,** pp. 115–159, eds Karato, S.-i., Forte, A.M., Liebermann, R.C., Masters, G. & Stixrude, L., American Geophysical Union, Washington, DC.

Keskin, M., Pearce, J.A. & Mitchell, J.C., 1998. Volcano-stratigraphy and geochemistry of collision-related volcanism on the Erzurum-Kars Plateau, northeastern Turkey, *J. Volc. Geotherm. Res.,* **85,** 355–404.

Kocyigit, A. & Erol, O., 2001. A tectonic escape structure: Erciyes pull-apart basin, Kayseri, central Anatolia, Turkey, *Geodyn. Acta,* **14,** 133–145.

Le Pichon, X. & Angelier, J., 1979. The Hellenic arc and trench system: A key to the neotectonic evolution of the eastern Mediterranean area, *Tectonophysics,* **60,** 1–42.

McClusky, S. *et al.*, 2000. Global positioning system constraints on plate kinematics and dynamics in the eastern Mediterranean and Caucasus, *J. geophys. Res.,* **105,** 5695–5719.

McKenzie, D., 1972. Active tectonics of the Mediterranean region, *Geophys. J. R. astr. Soc.,* **30,** 109–185.

McKenzie, D., 1978. Active tectonics of the Alpine-Himalayan belt: The Aegean Sea and surrounding regions, *Geophys. J. R. astr. Soc.,* **55,** 217–254.

Mainprice, D. & Nicolas, A., 1989. Development of shape and lattice preferred orientations: application to the seismic anisotropy of the lower crust, *J. Struct. Geol.,* **11,** 175–189.

Mainprice, D., Barruol, G. & Ismail, W.B., 2000. The seismic anisotropy of the Earth's mantle: From single crystal to polycrystal, in, *Earth's Deep Interior: Mineral physics and tomography from the atomic to the global scale,* American Geophysical Union, Geophysical Monograph, Vol. 117, pp. 237–264, eds Karato, S.-i., Forte, A.M., Liebermann, R.C., Masters, G. & Stixrude, L., American Geophysical Union, Washington, DC.

Makris, J. & Vees, R., 1977. Crustal structure of the central Aegean Sea and the islands of Evia and Crete, obtained by refractional seismic experiments, *J. Geophys.,* **42,** 329–341.

Menke, W.H. & Richards, P.G., 1980. Crust-mantle whispering gallery phases: A deterministic model of teleseismic Pn wave propagation, *J. geophys. Res.,* **85,** 5416–5422.

Paige, C.C. & Saunders, M.A., 1982. LSQR: Sparse linear equations and least squares problem, *ACM Trans. Math. Software,* **8,** 195–209.

Sandvol, E. *et al.*, 2001a. Tomographic imaging of Lg and Sn propagation in the Middle East, *Pure appl. Geophys.,* **158,** 1121–1163.

Sandvol, E. *et al.*, 2001b. Crustal and upper mantle seismic velocity structure in eastern Anatolia: results from the eastern Turkey PASSCAL seismic experiment, *Eos, Trans. Am. geophys. Un.,* **82,** 47.

Sato, H., Sacks, I.S. & Murase, T., 1989. The use of laboratory data for estimating temprature and partial melt fraction in the low velocity zone: Comparison with heat flow and electrical conductivity studies, *J. geophys. Res.,* **94,** 5689–5704.

Savage, M.K., 1999. Seismic anisotropy and mantle deformation: What have we learned from shear wave splitting?, *Rev. Geophys.,* **37,** 65–106.

Sengor, A.M.C. & Yilmaz, Y., 1981. Tethyan evolution of Turkey: a plate tectonic approach, *Tectonophysics,* **75,** 181–241.

Sengor, A.M.C., Gorur, N. & Sargolu, F., 1985. Strike-slip faulting and related basin formation in zones of tectonic escape: Turkey as a case study, in, *Strike-slip faulting and basin formation, Soc. Econ.*

Paleontol. Mineral., Special Publication, Vol. 37, pp. 227–264, eds Biddle, K.T. & Christie-Blick, N., *Soc. Econ. Paleontol. Mineral*, Oklahoma, USA.

Silver, P.G. & Chan, W.W., 1988. Implication for continental structure and evolution from seismic anisotropy, *Nature,* **335,** 34–39.

Smith, G.P. & Ekstrom, G., 1999. A global study of Pn anisotropy beneath continents, *J. geophys. Res.,* **104,** 963–980.

Snyder, D. & Barazangi, M., 1986. Deep crustal structure and flexure of the Arabian plate beneath the Zagros collisional mountain belt as inferred from gravity observations, *Tectonics,* **5,** 361–373.

Sonder, L.J. & England, P.C., 1989. Effects of a temperature-dependent rheology on large-scale continental extension, *J. geophys. Res.,* **94,** 7603–7619.

Takin, M., 1972. Iranian Geology and continental drift in the Middle East, *Nature,* **235,** 147–150.

Walker, D., 1977. High-frequency Pn phases observed in the Pacific at great distances, *Science,* **19,** 257–259.

Yilmaz, Y., 1990. Comparison of young volcanic associations of western and eastern Anatolia formed under a compressional regime: a review, *J. Volc. Geotherm. Res.,* **44,** 69–87.